Chemical Engineering Journal 165 (2010) 133–141

Contents lists available at ScienceDirect

Chemical Engineering Journal

journal homepage: www.elsevier.com/locate/cej

Modeling adsorption rate of pyridine onto granular activated carbon

R. Ocampo-Perez [a,b], R. Leyva-Ramos [a,*], P. Alonso-Davila [a], J. Rivera-Utrilla [b], M. Sanchez-Polo [b]

[a] Centro de Investigacion y Estudios de Posgrado, Facultad de Ciencias Quimicas, Universidad Autonoma de San Luis Potosi, Av. Dr. M. Nava No. 6, San Luis Potosi, SLP 78210, Mexico
[b] Departamento de Quimica Inorganica, Facultad de Ciencias, Universidad de Granada, 18071, Granada, Spain

ARTICLE INFO

Article history:
Received 15 June 2010
Received in revised form 1 September 2010
Accepted 2 September 2010

Keywords:
Activated carbon
Adsorption rate
Pyridine
Surface diffusion

ABSTRACT

The overall adsorption rate of pyridine on a granular activated carbon (GAC) is modeled in this work. The concentration decay curves for pyridine adsorption on GAC were obtained in a rotating basket adsorber. The experimental data were interpreted using a diffusional model that considered external mass transport, intraparticle diffusion, and adsorption on an active site; intraparticle diffusion could be due to both pore volume and surface diffusion. Results showed that the surface diffusion represented more than 93.5% of total intraparticle diffusion, confirming that surface diffusion was the mechanism controlling the overall adsorption rate. The model considering that surface diffusion was the controlling diffusion mechanism, interpreted reasonably well the concentration decay data for pyridine adsorption at different experimental conditions. Results showed that the surface diffusion coefficient increased while raising the temperature and mass of pyridine adsorbed at equilibrium, and was independent on the particle diameter. The external mass transport did not affect the overall rate of pyridine adsorption on GAC.

1. Introduction

Pyridine is a colorless, volatile, flammable, and toxic organic liquid that gives off an unpleasant odor when present in wastewater. Pyridine is widely used as a solvent in paints and an intermediate in the manufacture of insecticides, herbicides, textiles, fuels, drugs, vitamins, colorants, and adhesives. Due to its wide range of applications, its presence in wastewater has increased over the past years [1–3]. Pyridine and its derivatives are very toxic for aquatic and human life [2], and their removal is of great consequence to prevent diseases and avoid environmental pollution.

The most common methods for removal of pyridine from aqueous solution encompass biological degradation [4–6], photocatalysis [7], ozonation [8], membrane separation [9], and adsorption [3,10–13]. Adsorption on activated carbon has been widely applied to remove organic compounds from water effluents.

It has been shown that pyridine can be considerably adsorbed on activated carbon from an aqueous solution. Lataye et al. [11] investigated the adsorption of pyridine on rice husk ash and commercial granular activated carbon (GAC) and found that the percentage removal of pyridine was dependent on the solution pH, the maximum percentage removal happened at pH 6.5 with a carbon mass to solution volume ratio of 30 g/L, adsorption equilibrium was attained in 12 h and the adsorption process was endothermic.

Few works have been focused in the overall adsorption rate of pyridine on GAC and in the mass transport mechanisms controlling it. Mohan et al. [3] studied the adsorption kinetics of pyridine on activated carbons manufactured from agricultural waste and reported that the first-order kinetic model satisfactorily fitted the kinetic data.

The main aim of the present work was to study the overall adsorption rate of pyridine from aqueous solution on GAC and to develop a diffusional model to satisfactorily interpret the overall rate of adsorption. Furthermore, the effect of impeller speed, temperature, mass of adsorbent and initial concentration of pyridine upon the overall adsorption rate was analyzed in detail.

2. Diffusional model

It is well documented that the overall rate of adsorption rate on a porous solid includes the following three simultaneous steps: external mass transport, intraparticle diffusion, and adsorption on an active site; intraparticle diffusion may be due to pore volume diffusion, surface diffusion, or a combination of both mechanisms [14–16].

In this work, the diffusional model was derived by assuming the following: (i) intraparticle diffusion occurs by pore volume diffusion (Fick's diffusion) and surface diffusion, (ii) the rate of adsorption on an active site is instantaneous, and (iii) GAC particles are spherical. Model equations and initial and boundary conditions

* Corresponding author. Tel.: +52 4448132157; fax: +52 4448262449.
E-mail address: rlr@uaslp.com (R. Leyva-Ramos).

1385-8947/$ – see front matter © 2010 Elsevier B.V. All rights reserved.
doi:10.1016/j.cej.2010.09.002

Nomenclature

a	Prausnitz–Radke isotherm constant (L/g)
b	Prausnitz–Radke isotherm constant ($mg^{-\beta}\,L^{\beta}$)
C_A	concentration of pyridine in aqueous solution (mg/L)
C_{A0}	initial concentration of pyridine in aqueous solution (mg/L)
C_{Ar}	concentration of pyridine within the particle at distance r (mg/L)
$C_{Ar\|r=R_p}$	concentration of pyridine at the external surface of the particle at $r = R_p$ (mg/L)
d_p	average pore diameter (nm)
D_{AB}	molecular diffusion coefficient at infinite dilution (cm^2/s)
D_{eP}	effective pore volume diffusion coefficient (cm^2/s)
D_s	surface diffusion coefficient (cm^2/s)
D_{s0}	frequency factor of the surface diffusion coefficient (cm^2/s)
D_{Sq}	constant of Eq. (18) (cm^2/s)
E_S	activation energy for surface diffusion (kJ/mol)
k_L	external mass transfer coefficient in liquid phase (cm/s)
m	mass of adsorbent (g)
q	mass of pyridine adsorbed (mg/g)
q_{exp}	experimental mass of pyridine adsorbed (mg/g)
q_{pred}	mass of pyridine adsorbed predicted with the isotherm model (mg/g)
r	radial distance (cm)
R_p	radius of the particle (cm)
R	universal gas constant
SV	surface area per adsorbent mass unit (m^2/g)
S	external surface area per mass of adsorbent (cm^2/g)
T	temperature (K)
V	volume of the solution (mL)

Greek symbols

α	constant of Eq. (18) (g/mg)
β	Prausnitz–Radke isotherm constant
ε_p	void fraction of GAC particles
η_B	viscosity of water (cp)
ρ_p	density of adsorbent particles (g/mL)
τ	tortuosity factor
ϕ_A	dimensionless concentration of pyridine in the solution
ϕ_{exp}	experimental dimensionless concentration of pyridine in the solution
ϕ_{pred}	dimensionless concentration of pyridine in the solution predicted with the diffusional models

are [15,16]:

$$V\frac{dC_A}{dt} = -mSk_L(C_A - C_{Ar|r=R_p}) \quad (1)$$

$$t = 0, \quad C_A = C_{A0} \quad (2)$$

$$\varepsilon_p\frac{\partial C_{Ar}}{\partial t} + \rho_p\frac{\partial q}{\partial t} = \frac{1}{r^2}\frac{\partial}{\partial r}\left[r^2\left(D_{ep}\frac{\partial C_{Ar}}{\partial r} + D_s\rho\frac{\partial q}{\partial r}\right)\right] \quad (3)$$

(4) $C_{Ar} = 0,\ t = 0,\ 0 \le r \le R_p$

$$\left.\frac{\partial C_{Ar}}{\partial t}\right|_{r=0} = 0 \quad (5)$$

$$\left.D_{ep}\frac{\partial C_{Ar}}{\partial r}\right|_{r=R} + D_S\rho_p\frac{\partial q}{\partial r} = k_L(C_A - C_{Ar|r=R_p}) \quad (6)$$

If the rate of adsorption on an active site is instantaneous, there is local equilibrium between the pyridine concentration in the solution inside the pore and the mass of pyridine adsorbed on the pore surface. This equilibrium is normally represented by the adsorption isotherm, which is the mathematical relationship between C_{Ar} and q:

$$q = f(C_{Ar}) \quad (7)$$

The model represented by Eqs. (1)–(6) is the general diffusional model (PVSDM). The parameters k_L, D_s, and D_{ep} correspond to external transport, surface diffusion, and pore volume diffusion mechanisms, respectively. The general model can be simplified considering that the sole intraparticle diffusion mechanism may be either pore volume diffusion (PVDM) ($D_{ep} \neq 0, D_s = 0$) or surface diffusion (SDM) ($D_{ep} = 0, D_s \neq 0$).

The coupled partial and ordinary differential equations of the three diffusional models were solved numerically using the program PDESOL v2, which is based on the numerical method of lines [17].

3. Materials and methods

3.1. Adsorbent

The granular activated carbon (GAC) used in this work was manufactured from a bituminous carbon by Calgon, Inc. (Pittsburgh, PA) and is commercially available as F-400. The GAC was sieved to an average particle diameter of 1.02 mm, washed several times with deionized water, dried in an oven at 110 °C for 24 h and stored in a plastic container.

The surface area, pore volume and average pore diameter of GAC, determined by the N_2-BET method using a Micromeritics, model ASAP 2010, physisorption equipment, were $S_V = 925\ m^2/g$, $V_p = 0.534\ cm^3/g$, and $d_p = 2.2$ nm, respectively. The density of the solid, determined by the Helium displacement method using Micromeritics, model Accupic 1330, Helium pycnometer, was $\rho_s = 2.320\ g/cm^3$; the particle density and void fraction were $\rho_P = 1.036\ g/cm^3$ and $\varepsilon_p = 0.554$, respectively.

3.2. Determination of pyridine concentration in water solution

The pyridine concentration in an aqueous solution was determined by UV–visible spectroscopy. The absorbance of a pyridine solution was measured using a Shimadzu, model UV-160, spectrophotometer at a wavelength of 249.5 nm. The pyridine concentration of a sample was estimated with a calibration curve (absorbance vs. concentration) prepared with five standard pyridine solutions in a concentration range of 10–50 mg/L.

3.3. Adsorption equilibrium data

An Erlenmeyer flask of 500 mL was used as a batch adsorber to obtain the experimental adsorption equilibrium data of pyridine. A Nylon mesh bag containing a certain mass of GAC and a given volume of a pyridine solution were placed in the adsorber. The adsorber was partially submerged in a thermostatic water bath placed over a magnetic stirrer and the solution was stirred continuously with a Teflon coated stirring bar.

The experimental adsorption equilibrium data of pyridine on GAC were obtained by the following procedure. A Nylon mesh bag containing 1 g of GAC and 480 mL of a solution with a known initial concentration of pyridine at pH 10, were added in the

batch adsorber. The initial pyridine concentration was varied from 20 to 800 mg/L. The pyridine solution remained in contact with the GAC particles until equilibrium was reached; preliminary experiments revealed that three days were enough to attain equilibrium. The solution pH was measured periodically and kept constant by adding 0.01 and 0.1 M solutions of HCl and NaOH, as appropriate. After reaching equilibrium, the pyridine concentration in the solution was determined spectrophotometrically and the mass of pyridine adsorbed at equilibrium was calculated by a mass balance of pyridine. In previous runs without GAC, it was demonstrated that pyridine did not adsorb on the Nylon bag.

3.4. Method for obtaining the rate of adsorption data

A rotating basket batch adsorber was used to obtain the experimental concentration decay curves for the pyridine adsorption on GAC. This adsorber was composed of a 1 L three-neck reaction flask and an impeller with its blades replaced with stainless steel baskets. A pyridine solution was poured in the adsorber and the GAC particles were placed in the stainless steel mesh baskets, which were attached to a shaft connected to a variable speed motor. The adsorber was partially immersed in a constant temperature water bath controlled by a recirculator.

A pH 10 solution was prepared by mixing proper volumes of 0.01N HCl and NaOH solutions and a given volume (800–980 mL) of this solution was placed in the adsorber. A GAC mass (1–5 g) was added to the baskets, which were fastened to the impeller shaft, and then immersed in the pH 10 solution. The shaft was connected to the variable speed motor and the solution was mixed continuously by turning on the motor to a fixed rotating speed (100, 150 and 200 rpm), according to the experiment. The solution pH was measured periodically and kept constant by adding 0.01 and 0.1 N NaOH solutions, as required. The solution and GAC were left in contact until the temperature and pH remained constant. Subsequently, the stirrer was turned off and an aliquot of a solution of known concentration of pyridine at pH 10 was expeditiously poured into the adsorber solution to obtain the desired initial concentration. After the addition the total volume of the solution was 1 L. Right away, the impeller motor and the timer were turned on. The solution pH was monitored with a pH-meter and adjusted as indicated earlier. The total volume of NaOH solution added was always less than 2 mL and this volume represented 0.1% of the total volume. The solution was periodically sampled (5 mL) and analyzed to determine the pyridine concentration. Sampling times were 0, 1, 3, 5, 10, 15, 20, 25, 30, 40, 50, 60, 90, 120, 150, and 180 min. The total volume of the adsorber solution (1 L) was kept constant by adding 5 mL of a make-up solution immediately after sampling. The concentration of the make-up solution was the average of the initial concentration and the final concentration at equilibrium. The purpose of this addition was to replace the mass of pyridine withdrawn in the solution sample. Errors due to sampling and adding make-up solution were calculated by performing a mass balance and were always less than 2% in all experiments.

The experimental data, concentration of pyridine in solution versus time, were expressed in dimensionless form according to the following relationship:

$$\phi_A = \frac{C_A}{C_{A0}} \tag{8}$$

The dimensionless concentration, ϕ_A, was plotted against time to obtain the dimensionless concentration decay curve.

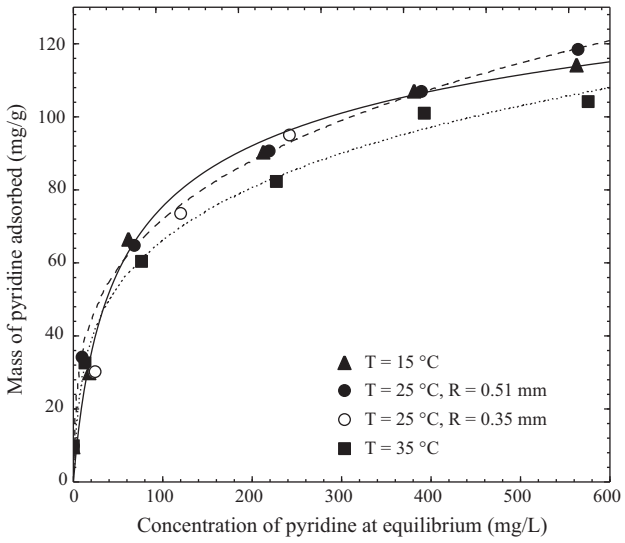

Fig. 1. Adsorption isotherms of pyridine on GAC at 15, 25, and 35 °C and pH 10. The lines represent the Prausnitz–Radke isotherm.

4. Results and discussion

4.1. Adsorption isotherm of pyridine on GAC

The effect of pH upon the adsorption of pyridine on activated carbon was investigated by evaluating the adsorption capacity of the GAC at an initial concentration of pyridine of 100 mg/L, T = 25 °C and the pH values ranging from 4 to 12. The pyridine adsorption capacity of the GAC was 16.5, 28.3, 30.3, 31.0, 32.2, 28.8 and 27.7 mg/g at the pH values of 4, 6, 8, 9, 10, 11 and 12, respectively. The maximum capacity of GAC for adsorbing pyridine took place at pH 10; however, the variation of the adsorption capacity was slight in the pH range 8–11. Similar results have been reported in previous works [3]. From the above, the adsorption kinetics was studied at pH 10.

Fig. 1 depicts the experimental adsorption equilibrium data at pH 10 and temperatures of 15, 25 and 35 °C. No significant differences in the data were observed at temperatures of 15 and 25 °C; however, the adsorption capacity of GAC was slightly decreased when the temperature was raised from 25 °C to 35 °C. In contrast, Mohan et al. [3] reported that the capacity of an activated carbon for adsorbing pyridine increased with temperature. This result may be explained recalling that Mohan et al. [3] prepared their activated carbons from coconut shell and coconut fibers whereas a bituminous GAC was used in the present study.

At temperatures of 15, 25 and 35 °C, the experimental adsorption equilibrium data of pyridine on GAC were interpreted with the Prausnitz–Radke adsorption isotherm model. This model can be represented by the following equation:

$$q = \frac{aC}{1 + bC^{\beta}} \tag{9}$$

The adsorption constants (Table 1) were evaluated by using a non-linear estimation method with Statistica software. The values of the isotherm constants as well as the average absolute percent-

Table 1
Constants of Prausnitz–Radke adsorption isotherm at pH 10.

T (°C)	a (L/g)	b (mg$^{-\beta}$ L$^{\beta}$)	β	%D
15	3.03	0.05	0.89	3.35
25	57.88	2.95	0.72	0.43
35	10.18	0.44	0.75	2.16

Table 2
Experimental conditions for pyridine concentration decay curves during adsorption on GAC at pH 10 and $R = 0.51$ mm.

Exp. No.	RPM	T (°C)	C_{A0} (mg/L)	m (g)	C_{Ae} (mg/L)	q_e (mg/g)	$k_L \times 10^3$ (cm/s)	$D_s \times 10^7$ (cm^2/s)
1	100	25	501.0	2.003	301.0	100.2	3.42	2.43
2	150	25	499.0	2.011	300.0	99.6	13.8	1.93
3	200	25	500.0	2.007	300.0	99.9	14.7	2.00
4	200	25	102.0	1.997	19.0	41.5	20.4	0.55
5	200	25	201.0	2.001	68.7	66.3	8.7	1.54
6	200	25	300.0	2.003	138.0	80.8	8.4	1.85
7	200	25	1011.0	2.012	753.0	129.4	10.4	3.77
8	200	25	499.0	1.000	392.0	108.2	14.3	2.70
9	200	25	499.0	2.994	226.0	91.3	11.1	2.02
10	200	25	499.0	4.011	166.0	83.4	9.28	2.08
11	200	25	499.0	5.001	117.0	76.6	9.18	1.77
12	200	15	499.4	2.002	294.0	102.8	13.7	1.62
13	200	15	300.0	2.011	122.0	88.8	7.7	1.16
14	200	15	100.0	1.994	16.5	41.7	21.4	0.46
15	200	35	499.4	2.009	307.0	96.7	4.92	3.14
16	200	35	304.2	2.002	149.5	77.4	7.5	2.94
17	200	35	100.0	1.998	19.3	40.3	18.3	0.69

age deviations are given in Table 1. The percentage deviations were calculated with the following equation:

$$\%D = \frac{1}{N}\sum_{i=1}^{N}\left|\frac{q_{\text{exp}} - q_{\text{pred}}}{q_{\text{exp}}}\right| \times 100\% \quad (10)$$

The Prausnitz–Radke isotherm and the adsorption equilibrium data are graphed in Fig. 1. The percentage deviations were less than 3.4% indicating that the Prausnitz–Radke fitted reasonably well the adsorption equilibrium data.

The effect of the particle diameter on the adsorption capacity was also investigated by obtaining the adsorption equilibrium data at the particle diameters of 1.02 and 0.7 mm. The results are shown in Fig. 1, and it can be noted that the adsorption capacity was independent on the particle diameter. This result was expected since the surface area of GAC was not influenced by the particle diameter.

4.2. Experimental concentration decay curves of pyridine

During the rate of adsorption experiments, it was observed that the solution pH decreased slightly and continuously. If the solution pH was not kept constant, the adsorption equilibrium would be varying with time. This is the reason all the adsorption rate experiments were carried out at a constant pH 10 and the solution pH was adjusted by adding 0.01 and 0.1N NaOH solutions. The operating conditions for all the concentration decay curves are given in Table 2.

4.3. Calculation of mass transport parameters

An experimental value of the molecular diffusivity of pyridine in an aqueous solution at infinite dilution was reported to be $D_{AB} = 0.58 \times 10^{-5}$ cm^2/s at 15 °C [18] and D_{AB} was estimated at the temperatures of 25 and 35 °C by using the following relationship between D_{AB} and temperature [18]:

$$D_{AB} \propto \frac{T}{\eta_B} \quad (11)$$

The molecular diffusivities were 0.77×10^{-5} and 0.98×10^{-5} cm^2/s at the temperatures of 25 and 35 °C, respectively.

The external mass transfer coefficient was assessed by the procedure proposed by Furusawa and Smith [19], based on the fact that when $t \to 0$ then $C_{Ar} \to 0$ and $C_A \to C_{A0}$. Substituting these conditions in Eq. (1), the following equation can be derived:

$$\left[\frac{d(C_A/C_{A0})}{dt}\right]_{t=0} = \frac{-mSk_L}{V} \quad (12)$$

The term in the right of Eq. (12) is the slope of the concentration decay at $t = 0$ and was estimated by using the first two data points of the concentration decay curve, at $t = 0$ and $t = 1$ min. The values of k_L estimated with Eq. (12) are given in Table 2 and ranged from 3.42×10^{-3} to 21.4×10^{-3} cm/s. These values are within the range of k_L values reported by other authors for rotating basket adsorbers [14,20].

4.4. Pore volume diffusion model (PVDM)

The relationship between the effective diffusion coefficient, D_{ep}, in a porous material and the molecular diffusivity, D_{AB}, can be described by various models. The simplest and commonly used model is based on the tortuosity factor, τ. In this model D_{ep} can be estimated from the following equation [21–23]:

$$D_{ep} = \frac{D_{AB}\varepsilon_p}{\tau} \quad (13)$$

Leyva-Ramos and Geankoplis [14] studied the intraparticle diffusion of several organic compounds in the same GAC used in this work. These authors found that τ varied between 3 and 4.6, and recommended using $\tau = 3.5$ for this activated carbon.

The experimental concentration decay curves were interpreted with the PVDM model and the mass transport parameters required for solving this model were D_{ep} and k_L. The D_{ep} was evaluated with Eq. (13) using $\tau = 3.5$ and $D_{AB} = 7.7 \times 10^{-6}$ cm^2/s, and the estimated value was $D_{ep} = 1.22 \times 10^{-6}$ cm^2/s at 25 °C. As indicated earlier, the k_L was evaluated using Eq. (12). In Fig. 2 is depicted the experimental concentration decay data for Exp. No. 3 and the concentration decay curve predicted with the PVDM model using $D_{ep} = 1.22 \times 10^{-6}$ cm^2/s and $\tau = 3.5$. As it can be seen in this figure, the PVDM model did not interpret the data and clearly overestimated the concentration decay curve. The time to reach equilibrium predicted by PVDM was 2400 min, but the experimental value was 120 min (Fig. 2). Thus, the experimental overall adsorption rate was 20 times higher than the overall rate of adsorption predicted by the PVDM model. This implied that the PVDM model can be fitted to the experimental data by increasing D_{ep}.

The effect of the size of the pyridine molecule (0.70 nm × 0.64 nm × 0.30 nm) relative to the average pore diameter would reduce D_{ep}. This effect is commonly known as restricted diffusion and was not taken into consideration for estimating D_{ep} [24].

To find the value of D_{ep} that best fitted the experimental data, the numerical solution of the PVDM model was matched with the concentration decay data. The optimal value of D_{ep} was evaluated

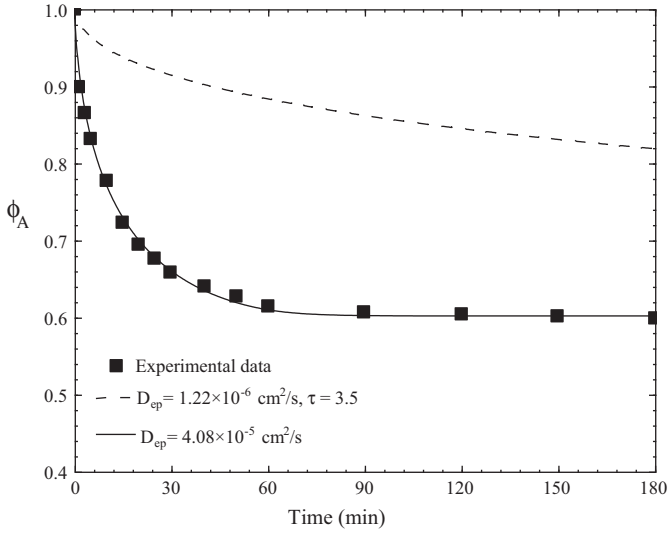

Fig. 2. Concentration decay curve for pyridine adsorption on GAC. The lines represent the PVDM model prediction. Exp. No. 3.

by minimizing the following objective function:

$$\text{Minimum} = \sum_{1}^{N} (\phi_{\text{exp}} - \phi_{pred})^2 \tag{14}$$

The optimal value of D_{ep} was 4.08×10^{-5} cm^2/s. The curve predicted with the PVDM model and this D_{ep} value is depicted in Fig. 2, which shows that the PVDM model fitted the experimental data reasonably well. However, the optimal D_{ep} value was approximately 5 times greater than the molecular diffusion coefficient of pyridine in water. This means that the pyridine molecules diffused much faster within the GAC pore volume than in the aqueous solution outside the pores. Obviously, this result is impossible because D_{ep} must always be lower than the molecular diffusion coefficient. It can be inferred that the intraparticle diffusion of pyridine in the GAC was not solely due to the pore volume diffusion, but another mechanism would have to be considered.

4.5. Pore volume and surface diffusion model (PVSDM)

The PVSMD model considered that intraparticle diffusion was due to both pore volume and surface diffusion mechanisms. In order to solve the PVSDM model, k_L was calculated from Eq. (12) and D_{ep} was evaluated with Eq. (13) assuming that $\tau = 3.5$. Hence, the surface diffusion coefficient, D_s, was the only unknown parameter and was evaluated by fitting the numerical solution of the PVSDM model to the concentration decay data. Again, the optimal value of D_s was obtained by minimizing Eq. (14). Fig. 3 depicts the experimental concentration decay data for Exp. No. 3, and the concentration decay curve predicted with the PVSDM model using the optimal value of $D_s = 1.93 \times 10^{-7}$ cm^2/s, showing that this model fitted the experimental data very satisfactorily.

It is very important to mention that it is a common practice to neglect pore volume diffusion when surface diffusion is taking place. However, this assumption had not been substantiated in many works reported in the literature of adsorption kinetics in the liquid phase. In order to evaluate the relative contribution of each diffusion mechanism to the overall intraparticle diffusion of pyridine, the mass transport due to pore volume diffusion, N_{AP}, and surface diffusion, N_{AS}, were estimated by the following equations:

$$N_{AP} = -D_{ep} \frac{\partial C_{Ar}}{\partial r} \tag{15}$$

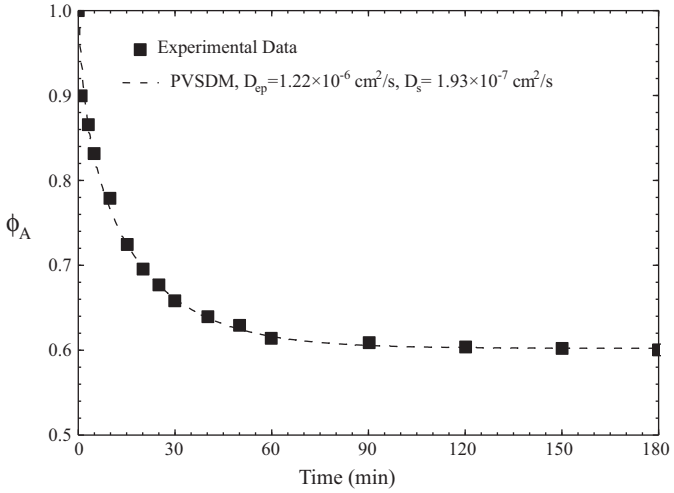

Fig. 3. Concentration decay curve for pyridine adsorption on GAC. The line represents the PVSDM model prediction. Exp. No. 3.

$$N_{AS} = -D_s \rho_p \frac{\partial q}{\partial r} \tag{16}$$

The relative contribution of surface diffusion to the overall intraparticle diffusion was estimated using the following equation:

$$\frac{N_{AS}}{N_{AS} + N_{AP}} = \frac{D_s \rho_p \, \partial q/\partial r}{D_s \rho_p \, \partial q/\partial r + D_{ep} \, \partial C_{Ar}/\partial r} \tag{17}$$

The relative contribution of surface diffusion with respect to time at different dimensionless radial positions $\xi(r/R)$ is plotted in Fig. 4. The results revealed that the contribution of surface diffusion always represented over 93.5% of the overall intraparticle diffusion, regardless of the radial position and time. Hence, the intraparticle diffusion of pyridine during adsorption on GAC was predominantly due to surface diffusion.

The importance of surface diffusion can be partly attributed to the difference in the concentration gradients in the solution and on the surface of the GAC. The concentration of pyridine in the solution ranged up to 1000 mg/L or 1 mg/mL, and the concentration of pyridine adsorbed on the GAC varied up to 100 mg/g or 103.6 mg/mL. This last value was calculated using the density of the particle, $\rho_P = 1.036$ g/cm^3. In other words, the concentration in the adsorbed phase was 100 times greater than that in the solution.

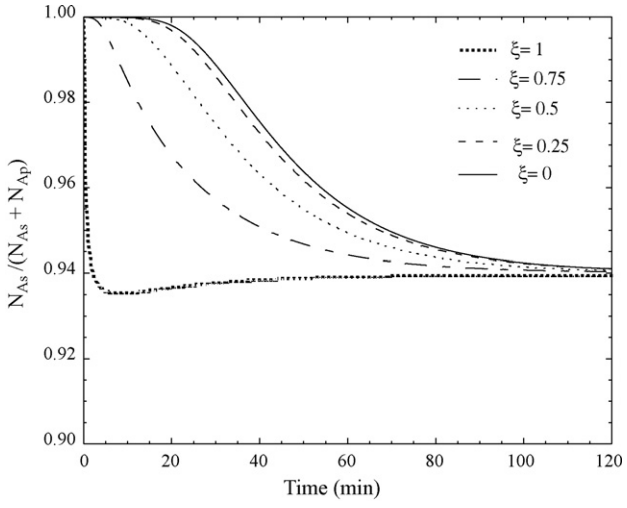

Fig. 4. Contribution of surface diffusion to the intraparticle diffusion at different radial positions. Exp. No. 3.

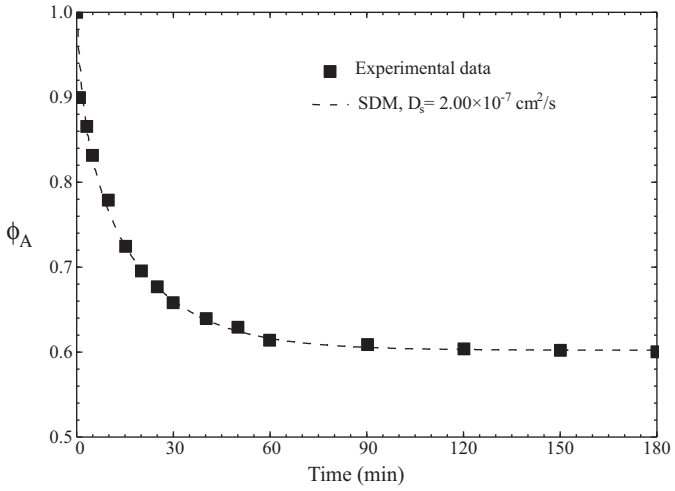

Fig. 5. Concentration decay curve for pyridine adsorption on GAC. The line represents the SDM model prediction. Exp. No. 3.

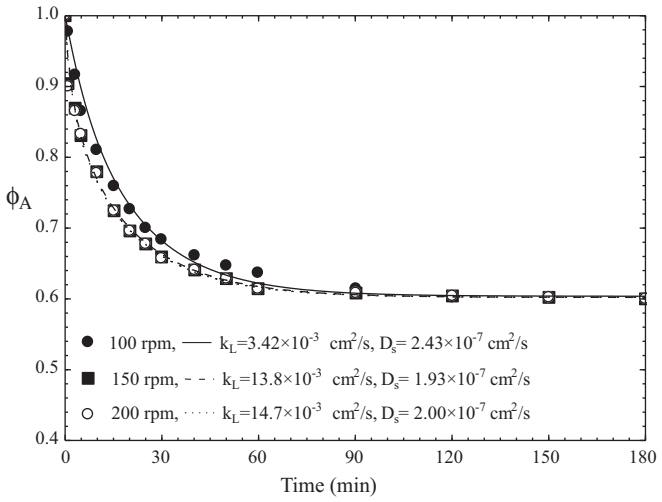

Fig. 6. Effect of the rotating speed on the concentration decay curves for pyridine adsorption on GAC. The lines represent the SDM model predictions. Exp. Nos. 1–3.

4.6. Surface diffusion model (SDM)

According to the SDM model, the intraparticle diffusion is exclusively due to surface diffusion and pore volume diffusion can be neglected ($N_{AS} \gg N_{AP}$). The mass transfer parameters of the SDM model are k_L and D_s, and as described in Section 4.3, k_L was estimated with Eq. (12). The value of D_s was assessed by matching the numerical solution of the SDM model with the experimental concentration decay data. The best value of D_s was obtained by minimizing the objective function described by Eq. (14). Fig. 5 shows the concentration decay curve predicted with the SDM model and the optimal value of $D_s = 2.00 \times 10^{-7}$ cm^2/s. As shown, the SDM model fitted the experimental data reasonably well. It is worth mentioning that the value of D_s in the SDM model ($D_s = 2.00 \times 10^{-7}$ cm^2/s) is 3.5% higher than the D_s of the PVSDM model ($D_s = 1.93 \times 10^{-7}$ cm^2/s), confirming that the contribution of surface diffusion was much greater than that of pore volume diffusion.

Therefore, it was considered that the adsorption rate of pyridine on GAC can be satisfactorily interpreted with the SDM model. From the above the SDM was used in the latter sections of this work.

Few studies have been carried out about surface diffusion in GAC. Traegner and Suidan [25] applied a diffusional model to the experimental data of p-Nitrophenol adsorption kinetics on activated carbon F-400, and obtained a value of $D_s = 1.92 \times 10^{-8}$ cm^2/s, which is an order of magnitude lower than that found in the present study. Ganguly and Goswami [26] fitted a diffusional model to the experimental concentration decay data for acetic acid adsorption on a GAC and demonstrated that D_s for acetic acid ranged from 6×10^{-7} to 8.5×10^{-7} cm^2/s. McKay and Duri [27] studied the adsorption rate of two basic dyes (Basic Red 22 and Basic Yellow 21) on the activated carbon F-400 and reported $D_s = 1.3 \times 10^{-11}$ cm^2/s and $D_s = 8.5 \times 10^{-11}$ cm^2/s, respectively. The adsorption rate of methylene blue on activated carbon prepared from palm kernel shell was satisfactorily interpreted using a film-concentration dependent surface diffusion model and the values of D_s at zero surface coverage ranged from 1.03×10^{-10} to 7.03×10^{-10} cm^2/s [16]. In a study about the adsorption rate of pentachlorophenol (PCP) on a bituminous GAC, Leyva-Ramos et al. [20] demonstrated that the intraparticle diffusion of PCP was mainly controlled by surface diffusion, which was dependent on the mass of PCP adsorbed at equilibrium.

4.7. Effect of mass external transport upon overall adsorption rate

In a rotating basket adsorber, the external mass transport depends on the impeller speed, particle size, and adsorber geometry. Fig. 6 depicts the concentration decay curves of pyridine at rotating speeds of 100, 150 and 200 rpm (Exp. Nos. 1–3). It can be noted that the concentration decay curves at 150 and 200 rpm are below the decay curve at 100 rpm, and the decay curve at 200 rpm is overlapping the decay curve at 150 rpm. Furthermore, the time required to reach equilibrium was 90, 90 and 120 min for rotating speeds of 200, 150 and 100 rpm, respectively. In other words, the overall adsorption rate increased 1.33 times (120/90) when the rotating speed was increased from 100 to 150 rpm, but did not vary augmenting the speed from 150 to 200 rpm. Moreover, k_L increased 4-fold (from 3.42×10^{-3} to 13.8×10^{-3} cm/s) and 1.07-fold (from 13.8×10^{-3} to 14.7×10^{-3} cm/s) when the rotating speed increased from 100 to 150 rpm and from 150 to 200 rpm, respectively. Hence, the external mass transport did not affect the overall adsorption rate at rotating speeds faster than 150 rpm. Thereupon, the rest of experiments were carried out at a rotating speed of 200 rpm.

4.8. Effect of the mass of pyridine adsorbed on the surface diffusion coefficient

The effect of the mass of pyridine adsorbed at equilibrium, q_e, on D_s was studied by varying the initial concentration of pyridine and keeping constant the mass of GAC or by changing the mass of GAC and maintaining constant the initial concentration of pyridine. For a GAC mass of 2, Fig. 7 depicts the concentration decay curves at the initial concentrations of 100, 200, 300, 500, and 1000 mg/L (Exp. Nos. 3–7) and the corresponding q_e values of 41.5, 66.3, 80.8, 99.9, and 129.4 mg/g, respectively. This figure shows that the SDM model interpreted the experimental data reasonably well and that D_s increases with q_e. At an initial pyridine concentration of 500 mg/L, the concentration decay curves were obtained for the GAC quantities of 1, 2, 3, 4, and 5 g (Exp. Nos. 3, 8–11) and the corresponding q_e values were 108.15, 99.92, 91.33, 83.43, and 76.55 mg/g, respectively. The concentration decay curves for Exp. Nos. 3, 8–11 were not presented because they showed the same behavior as that depicted in Fig. 7. Besides, the SDM model satisfactorily interpreted the experimental data and D_s increased rising q_e (Table 2).

Do [21], Leyva-Ramos et al. [20] and Suzuki [23] have reported that surface diffusion was the most important intraparticle diffu-

Table 3
Values of the frequency factor and activation energy for surface diffusion.

Exp. No.	T (K)	q_e (mg/g)	$\bar{q}_e$ (mg/g)	$D_s \times 10^7$ (cm^2/s)	D_{s0} (cm^2/s)	E_s (kJ/mol)
12	288	102.8	99.8	1.62	0.012	27.62
3	298	99.9		2.00		
15	308	96.7		3.14		
13	288	88.8	82.3	1.16	0.011	27.08
6	298	80.8		1.85		
16	308	77.4		2.94		
14	288	41.7	41.2	0.46	0.033	33.17
4	298	41.5		0.55		
17	308	40.3		0.69		

sion mechanism in adsorbents with a large surface area (activated carbons) and that D_S increased with the mass of solute adsorbed.

The values of D_S in Table 2 clearly showed that D_S increased with q_e. A possible explanation for this trend was that the pyridine molecules were initially adsorbed on sites, which required higher adsorption energy and very few of the adsorbed molecules have enough energy to be desorbed from a site and diffuse to another adsorption site. Once the sites with higher adsorption energy were occupied, afterwards the pyridine molecules were adsorbed on sites with lower adsorption energy so more pyridine molecules can be desorbed and move from one site to another, inferring that D_S was increasing with surface loading.

The relationship between D_S and q_e was interpreted with the following equation [28,29]:

$$D_s = D_{Sq} \exp(-\alpha q_e) \tag{18}$$

This equation can be linearly expressed by rearranging it as follows:

$$\ln D_s = \ln D_{Sq} - \alpha q_e \tag{19}$$

The values of D_{Sq} and α were estimated by a least-squares method and the best values were $D_{Sq} = 3.44 \times 10^{-8}$ cm^2/s and $\alpha = -0.0194$ g/mg. The effect of q_e on D_S is shown in Fig. 8 and illustrates the linear relationship between $\ln D_S$ and q_e. Except for one data point, Eq. (19) satisfactorily fitted the experimental data.

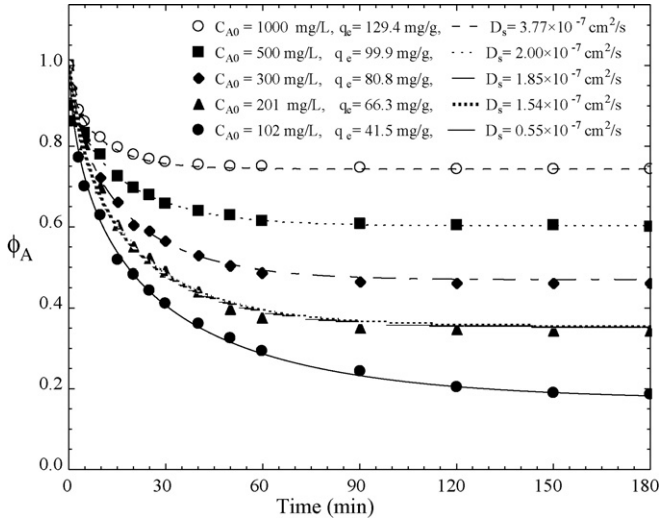

Fig. 7. Effect of the mass of pyridine adsorbed at equilibrium in the concentration decay curves for pyridine adsorption on GAC. The lines represent the SDM model predictions. Exp. Nos. 3–7.

4.9. Effect of temperature on the surface diffusion coefficient of pyridine

Various studies have reported that the dependence of D_S on temperature can be interpreted with the following equation [30]:

$$D_s = D_{s0} \exp\left(\frac{-E_S}{RT}\right) \tag{20}$$

The effect of temperature on D_S was investigated by obtaining concentration decay data at temperatures of 15, 25, and 35 °C and at the initial concentrations of 500, 300, and 100 mg/L (Exp. Nos. 3, 4, 6, 12–17). The mass of GAC in all these experiments was almost kept constant at 2 g. At a given initial concentration, it was observed that q_e varied slightly with temperature because the adsorption equilibrium was tenuously influenced by temperature. For example, at an initial concentration of 500 mg/L, the values of q_e were 102.8, 99.9 and 96.7 mg/g for the temperatures of 15, 25, and 35 °C, respectively (Exp. Nos. 12, 3 and 15). The q_e values for these experiments were averaged since D_S was found to be dependent upon q_e. The values of the average mass of pyridine adsorbed, $\bar{q}_e$, are given in Table 3 for the initial concentrations of 500, 300 and 100 mg/L, respectively.

Fig. 9 shows the experimental concentration decay data at the temperatures of 15, 25, and 35 °C and the initial concentrations of 500 and 300 mg/L, and the concentration decay curves predicted with the SDM model. The SDM model satisfactorily interpreted the experimental data at different temperatures. The values of D_S given in Table 3 show that D_S was augmented 1.9, 2.5 and 1.5 times at $\bar{q}_e$ of 99.8, 82.3 and 41.2 mg/g, respectively, when the temperature was increased 20 °C. The effect of temperature on D_S is illustrated in Fig. 10. This behavior was attributed to the fact that the adsorbed pyridine molecules had greater internal energy when the temperature was increased. Hence, increasing the temperature, the

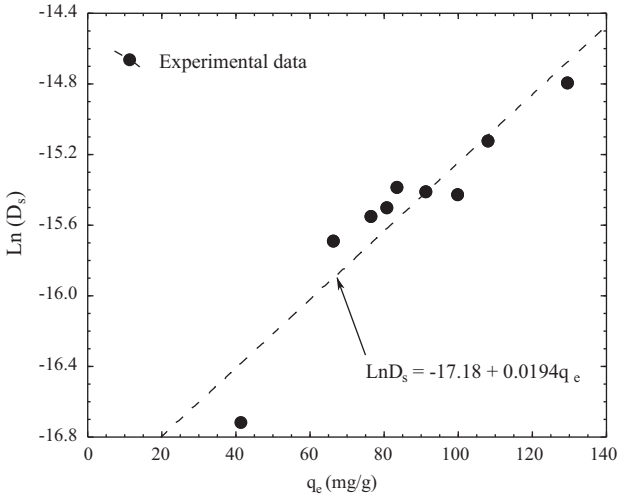

Fig. 8. Effect of the mass of pyridine adsorbed at equilibrium on D_S. Exp. Nos. 3–11.

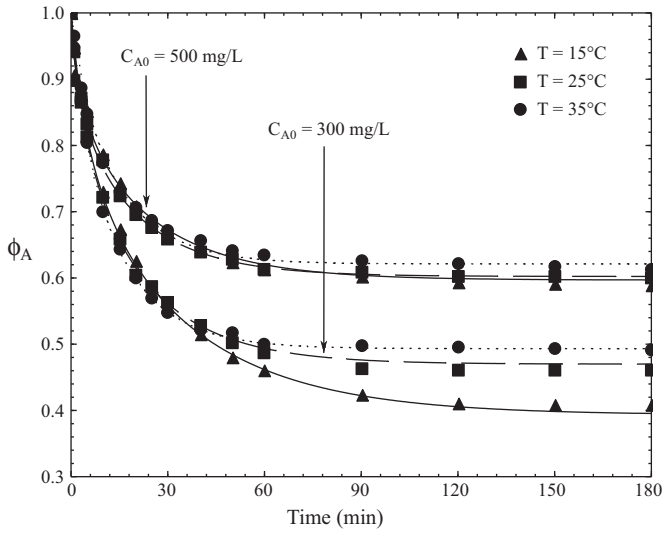

Fig. 9. Effect of temperature and mass of pyridine adsorbed at equilibrium on the concentration decay curves for adsorption of pyridine on GAC. The lines represent the SDM model predictions. Exp. Nos. 3, 6, 12, 13, 15, and 16.

adsorbed molecules of pyridine required less energy to be desorbed from a site and then diffused to another site.

At a constant $\bar{q}_e$, Eq. (20) was fitted to the experimental values of D_s at different temperatures (see Table 3). The constants D_{s0} and E_s were estimated by using a non-linear estimation method. The values of these constants are given in Table 3 and Eq. (20) is plotted in Fig. 10. As seen in this figure, the dependence of D_s on temperature can be well represented by an Arrhenius-typed equation, and the values of E_s and D_{s0} are within the range of values reported in the literature [31]

4.10. Effect of particle diameter on the surface diffusion coefficient

This effect was investigated by obtaining the adsorption rate data under the same experimental conditions but changing the particle diameter. The particle diameters tested in this work were 0.70 and 1.02 mm. It was noticed that the time to reach equilibrium was decreased from 120 to around 70 min while reducing the diameter of the particles from 1.02 to 0.70 mm, respectively. Hence, the overall adsorption rate increased 1.7 times when the diameter of the particle was diminished 1.5 times. This behavior was due to the overall adsorption rate of pyridine was controlled by intraparticle diffusion. If the particle diameter were smaller, then the pyridine molecule would diffuse a shorter distance from the external surface to the active sites inside the pores, resulting in a faster overall adsorption rate.

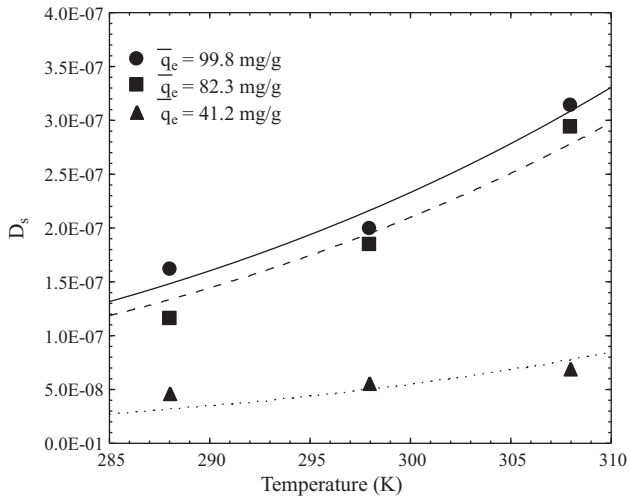

Fig. 10. Effect of temperature on D_s. The lines represent Eq. (20).

In this case the concentration decay data and the concentration decay curves predicted with the SDM model were not graphed because they exhibited the same trend as those presented in Figs. 3, 5 and 7. The SDM model satisfactorily predicted the concentration decay, and the D_s varied very slightly with the particle diameter, but D_s can be essentially considered independent on the particle diameter. In surface diffusion the molecules move along the surface of the pores hence D_s cannot be dependent on the particle size.

5. Conclusions

In a rotating basket adsorber, the external mass transport did not affect the overall adsorption rate of pyridine on GAC for rotating speeds above 150 rpm.

The PVDM model considering that pore volume diffusion was the controlling mechanism and surface diffusion was negligible, was reasonably well fitted to the experimental concentration decay data. However, D_{ep} values were much greater than the molecular diffusion coefficient of pyridine in water. Hence, the D_{ep} values assessed with the PVDM model were incorrect.

The PVSDM model assuming that pore volume and surface diffusion were both important in intraparticle diffusion, satisfactorily fitted the experimental data. In this model, D_{ep} was calculated by using the tortuosity factor equation ($\tau = 3.5$), and D_s was obtained by fitting the PVSDM model to the experimental data. The contribution of surface diffusion to intraparticle diffusion was calculated, showing that surface diffusion represented more than 93.5% of intraparticle diffusion. This finding confirmed that surface diffusion is the controlling mechanism of the overall rate of adsorption and pore volume diffusion can be neglected.

The SDM model considered that intraparticle diffusion was solely due to surface diffusion. The SDM modeled reasonably well the concentration decay data for pyridine adsorption on GAC at different experimental conditions. Furthermore, it was found that D_s was augmented by increasing q_e and T, and independent on particle diameter.

Acknowledgements

This study was funded by CONACyT through grant No. CB-2007-01-83375. In addition, FOMIX San Luis Potosi (FMSLP-2008-C02-106795) granted a fellowship to Mr. Raul Ocampo Perez to pursue a research internship in the Department of Inorganic Chemistry, University of Granada, Spain.

References

[1] G.D. Henry, De novo synthesis of substituted pyridines, Tetrahedron 60 (2004) 6043–6061.
[2] D.H. Lataye, I.M. Mishra, I.D. Mall, Removal of pyridine from aqueous solution by adsorption on bagasse fly ash, Ind. Eng. Chem. Res. 45 (2006) 3934–3943.
[3] D. Mohan, K.P. Singh, S. Sinha, D. Gosh, Removal of pyridine from aqueous solution using low cost activated carbons derived from agricultural waste materials, Carbon 42 (2004) 2409–2421.
[4] A.K. Mathur, C.B. Majumder, S. Chatterjee, P. Roy, Biodegradation of pyridine by the new bacterial isolates *S. putrefaciens* and *B. sphaericus*, J. Hazard. Mater. 157 (2008) 335–343.
[5] K.V. Padoley, A.S. Rajvaidya, T.V. Subbarao, R.A. Pandey, Biodegradation of pyridine in a completely mixed activated sludge process, Biores. Technol. 97 (2006) 1225–1236.
[6] L. Qiao, J. Wang, Microbial degradation of pyridine by *Paracoccus sp.* isolated from contaminated soil, J. Hazard. Mater. 176 (2010) 220–225.

[7] H. Zhao, S. Xu, J. Zhong, X. Bao, Kinetic study on the photo-catalytic degradation of pyridine in TiO_2 suspension systems, Catalysis Today 93–95 (2004) 857–861.
[8] R. Andreozzi, A. Insola, V. Caprio, M.G. D'Amore, Ozonation of pyridine in aqueous solution: mechanistic and kinetic aspects, Water Res. 25 (1991) 655–659.
[9] M.K. Mandal, P.K. Bhattacharya, Poly(ether-block-amide) membrane for pervaporative separation of pyridine present in low concentration in aqueous solution, J. Membrane Sci. 286 (2006) 115–124.
[10] M.E. Essington, Adsorption of pyridine by combusted oil shale, Environ. Geo. Water Sci. 19 (1992) 83–89.
[11] D.H. Lataye, I.M. Mishra, I.D. Mall, Pyridine sorption from aqueous solution by rice husk ash (RHA) and granular activated carbon (GAC): parametric, kinetic, equilibrium and thermodynamic aspects, J. Hazard. Mater. 154 (2008) 858–870.
[12] D. Mohan, K.P. Singh, S. Sinha, D. Gosh, Removal of pyridine derivatives from aqueous solution by activated carbons developed from agricultural waste materials, Carbon 43 (2005) 1680–1693.
[13] J. Ren, J. Wang, C. Huo, X. Wen, Z. Cao, S. Yuan, Y. Li, H. Jiao, Adsorption of NO, NO_2, pyridine and pyrrole on α-Mo2C(0 0 0 1): a DFT study, Surf. Sci. 601 (2007) 1599–1607.
[14] R. Leyva-Ramos, C.J. Geankoplis, Diffusion in liquid-filled pores of activated carbon. I. Pore volume diffusion, Can. J. Chem. Eng. 72 (1994) 262–271.
[15] R. Leyva-Ramos, C.J. Geankoplis, Model simulation and analysis of surface diffusion of liquids in porous solids, Chem. Eng. Sci. 40 (1985) 799–807.
[16] T.S.Y. Choong, T.N. Wong, T.G. Chuah, A. Idris, Film-pore-concentration-dependent surface diffusion model for the adsorption of dye onto palm kernel shell activated carbon, J. Colloid Interface Sci. 301 (2006) 436–440.
[17] W.E. Schiesser, C.A. Silebi, Computational Transport Phenomena. Numerical Methods for the Solution of Transport Problems, Cambridge University Press, Cambridge, UK, 1997.
[18] B.E. Poling, M. Prausnitz, J.P. O'Connell, The Properties of Gases and Liquids, 5th ed., McGraw-Hill, U. S. A., 2006.
[19] T. Furusawa, J.M. Smith, Fluid-particle and intraparticle mass transport rates in slurries, Ind. Eng. Chem. Fundam. 12 (1973).
[20] R. Leyva-Ramos, L.A. Bernal-Jacome, J. Mendoza-Barron, M.M.G. Hernandez-Orta, Kinetic modeling of pentachlorophenol adsorption onto granular activated carbon, J. Taiwan Inst. Chem. Eng. 40 (2009) 622–629.
[21] D.D. Do, Adsorption Analysis: Equilibria and Kinetics, 1st ed., Imperial College Press, London, UK, 1998.
[22] D.M. Ruthven, Principles of Adsorption and Adsorption Processes, 1st ed., Wiley, USA, 1984.
[23] M. Suzuki, Adsorption Engineering, 1st ed., Elsevier, Japan, 1990.
[24] R. Leyva-Ramos, P.E. Diaz-Flores, J. Leyva-Ramos, R.A. Femat-Flores, Kinetic modeling of pentachlorophenol adsorption from aqueous solution on activated carbon fibers, Carbon 45 (2007) 2280–2289.
[25] U.K. Traegner, M.T. Suidan, Parameter evaluation for carbon adsorption, J. Environ. Eng. 115 (1989) 109–128.
[26] S.K. Ganguly, A.N. Goswami, Surface diffusion kinetics in the adsorption of acetic acid on activated carbon, Sep. Sci. Technol. 31 (1996) 1267–1278.
[27] G. McKay, B.A. Duri, Multicomponent dye adsorption onto carbon using a solid diffusion mass-transfer model, Ind. Eng. Chem. Res. 30 (1991) 385–395.
[28] K.K.H. Choy, J.F. Porter, G. McKay, Film-surface diffusion during the adsorption of acid dyes onto activated carbon, J. Chem. Technol. Biotechnol. 79 (2004) 1181–1188.
[29] A.H. Mollah, C.W. Robinson, Pentachlorophenol adsorption and desorption characteristics of granular activated carbon II. Kinetics, Water Res. 30 (1996) 2907–2913.
[30] K. Miyabe, S. Takeuchi, Analysis of surface diffusion phenomena in liquid phase adsorption, J. Phys. Chem. B 101 (1997) 7773–7779.
[31] K. Miyabe, M. Suzuki, Mass-transfer phenomena on the surface of adsorbents in reversed-phase chromatography, Ind. Eng. Chem. Res. 33 (1994) 1792–1802.